jaa Just accepted article

EuroIntervention

**Title:** **Detection of Optical Coherence Tomography–Defined Thin-Cap Fibroatheroma in the Coronary Artery Using Deep Learning.**

**Authors:** Hyun-Seok Min, PhD; Ji Hyeong Yoo, BS; Soo-Jin Kang, MD; June-Goo Lee, PhD; Hyungjoo Cho, BS; Pil Hyung Lee, M.D; Jung-Min Ahn, M.D; Duk-Woo Park, M.D; Seung-Whan Lee, M.D; Young-Hak Kim, M.D; Cheol Whan Lee, M.D; Seong-Wook Park, M.D; Seung-Jung Park, M.D

**DOI:** 10.4244/EIJ-D-19-00487

**Citation:** Min HS, Yoo HJ, Kang SJ, Lee JG, Cho H, Lee PH, Ahn JM, Park DW, Lee SW, Kim YH, Lee CW, Park SW, Park SJ. Detection of Optical Coherence Tomography–Defined Thin-Cap Fibroatheroma in the Coronary Artery Using Deep Learning. *EuroIntervention* 2019; Jaa-677 2019, doi: 10.4244/EIJ-D-19-00487



**Manuscript submission date:** 15 May 2019

**Revisions received:** 01 July 2019, 16 September 2019, 09 October 2019

**Accepted date:** 07 November 2019

**Online publication date:** 12 November 2019

# Detection of Optical Coherence Tomography–Defined Thin-Cap Fibroatheroma in the Coronary Artery Using Deep Learning

Hyun-Seok Min, PhD[1], Ji Hyeong Yoo, BS[1], Soo-Jin Kang, MD[1]*, June-Goo Lee, PhD[2], Hyungjoo Cho, BS[1], Pil Hyung Lee, MD[1], Jung-Min Ahn, MD[1], Duk-Woo Park, MD[1], Seung-Whan Lee, MD[1], Young-Hak Kim, MD[1], Cheol Whan Lee, MD[1], Seong-Wook Park, MD[1], Seung-Jung Park, MD[1]

[1]Department of Cardiology, University of Ulsan College of Medicine, Asan Medical Center, Seoul, Korea, [2]Biomedical Engineering Research Center, Asan Institute for Life Sciences, Seoul, Korea



Total word count: 4931

Short title: Automatic detection of OCT-derived TCFA by deep learning

* **Correspondence:** Soo-Jin Kang, MD, PhD., Professor, Dept. of Cardiology, Asan Medical Center, University of Ulsan College of Medicine, 88, Olympic-ro 43-gil, Songpa-gu, Seoul 05505, Korea

Phone: +82-2-3010-3157, Fax: +82-2-475-6898, E-mail: sjkang@amc.seoul.kr

**Abstract**

**Aims.** To develop a deep learning model for classifying frames with vs. without optical coherence tomography (OCT)-derived thin-cap fibroatheroma (TCFA).

**Methods and Results**. Total 602 coronary lesions from 602 angina patients were randomized into training and test sets at a 4:1 ratio. A DenseNet model was developed to classify OCT frames with or without OCT-derived TCFA. Gradient-weighted class activation mapping was used to visualize the area of attention. In the training sample (35,678 frames of 480 lesions), the model with 5-fold cross-validation had an overall accuracy of 91.6±1.7%, sensitivity of 88.7±3.4%, and specificity of 91.8±2.0% (averaged AUC=0.96±0.01) in predicting the presence of TCFA. In the test samples (9,722 frames of 122 lesions), the overall accuracy at the frame level was 92.8% within the lesion (AUC=0.96) and 91.3% in the entire OCT pullback. The correlation between the %TCFA burdens per vessel predicted by the model compared with that identified by experts was significant ($r=0.87$, $p<0.001$). The region of attention was localized at the site of the thin cap in 93.4% of TCFA-containing frames. Total computational time per a pullback was 2.1 ± 0.3 seconds.

**Conclusion.** Deep learning algorithm can accurately detect an OCT-TCFA with a high reproducibility. The time-saving computerized process may assist clinicians to easily recognize high-risk lesions and to make decisions in the catheterization laboratory.

**Classification:** ACS/NSTE-ACS, Miscellaneous, plaque rupture, optical coherence tomography

**Condensed abstract**

A deep learning algorithm was developed to classify OCT frames with or without OCT-derived TCFA. The model showed the frame-level accuracy was 92.8% in the lesion (AUC=0.96) and 91.3% in the entire OCT pullback with 2.1 ± 0.3 seconds of a total computational time. Also, the model-predicted %TCFA burdens per vessel significantly correlated with that measured by experts (r=0.87, p<0.001). The region of attention was localized at the site of the thin cap in majority, which indicated that the model predicted TCFAs detecting a thin cap. The data-driven approach may assist clinicians in quickly assessing high-risk coronary lesions.

**Abbreviations**

TCFA= thin-cap fibroatheroma

OCT= optical coherence tomography

FCT= fibrous cap thickness

DenseNet= densely connected convolutional networks

ROC= receiver operating characteristic

AUC= area under curve

TP=true positive

FP= false positive

FN=false negative

DSC= Dice similarity coefficient

Grad-CAM= gradient-weighted class activation mapping

## Introduction

Thin-cap fibroatheroma (TCFA) is a precursor of plaque rupture with acute coronary thrombosis, and is characterized by an inflamed fibrous cap with a thickness < 65 μm, a large necrotic core, and an infiltration of foamy macrophages.[1-4] Previous studies on the natural history of deferred coronary lesions demonstrated that the presence of TCFA is an independent predictor of future adverse cardiac outcomes.[5,6] Moreover, TCFA-containing lesions were associated with a high risk of distal embolization and periprocedural myocardial infarction during percutaneous coronary intervention.[7,8] However, the majority of previous studies have conducted only qualitative assessments of TCFA (i.e., the presence or absence of TCFA within the target vessel), which poorly represents the status of the whole length of the vessel.

Currently, optical coherence tomography (OCT) is the only imaging modality with sufficient resolution (10–15 μm of spatial resolution) to measure fibrous cap thickness (FCT) and identify TCFA-containing lesions.[9-11] Although studies of FCT measurement ex vivo showed a good interobserver agreement relative to histology, its reproducibility in vivo remains poor.[12,13] Furthermore, the feature evaluated in the majority of these studies was not the extent of TCFA but rather the presence or absence of TCFA in any frame within a target vascular segment; this may not necessarily reflect the status of the entire vessel. Conversely, the quantification of TCFA by per-frame interpretation from whole OCT pullback is time consuming. Therefore, a standard interpretation algorithm is needed to reduce interobserver variation and the cost associated with OCT analysis.

Deep learning approaches have recently become dominant in various computer vision tasks such as classification, detection, and segmentation.[14-16] Convolutional

neural networks, which is a type of deep learning, is designed to automatically and adaptively ascertain the spatial hierarchies of features via backpropagation. This data-driven approach can be applied to develop prediction models for medical imaging with excellent performance. Previous studies have developed deep learning algorithms for automatic OCT segmentation, tissue classification, and atheroma detection.[17,18] Although these studies highlighted the importance of the approaches for the accurate and rapid interpretation of OCT, their clinical implication was limited by the inclusion of only a small number of OCT cases, the suboptimal accuracies, and the lack of an algorithm to identify a TCFA.

By using a larger OCT cohort (45,400 OCT frames in 602 coronary arteries), this current study was conducted to develop an end-to-end neural network model that can automatically classify frames with or without OCT-derived TCFA, as the prototype of vulnerable plaque.



## Methods

**Study population and data collection.** Between May 2010 and May 2016, 6598 consecutive patients with stable and unstable angina underwent invasive coronary angiography at Asan Medical Center, Seoul, South Korea. Pre-procedural OCT data were obtained in 798 patients at the discretion of the operators. All patients had at least one lesion with 30%–85% of angiographic stenosis. When multiple lesions were evaluated in one patient, the lesion with the highest degree of angiographic stenosis was selected. We excluded 171 stented lesions and 25 lesions because of poor imaging quality, and 602 coronary lesions from 602 patients were studied in total. Patients were randomly assigned into training (n = 480) or test (n = 122) sets at a ratio of 4:1. Per-

patient randomization was conducted to avoid adjacent frames with similar characteristics from being enrolled into both the training and test sets. Furthermore, data from a nonoverlapping population of 65 consecutive patients (with unselected 65 OCT pullback images acquired from the St. Jude OCT system) who underwent pre-procedural OCT between February 01, 2016, and November 30, 2017, were used for an additional validation study.

Clinical information was supported by the Asan Biomedical Research Environment system. All patients provided written informed consent. This study was approved by the institutional review board of Asan Medical Center.

After the intracoronary administration of 0.2 mg nitroglycerin, OCT images were acquired using a nonocclusive technique with the C7XR™ system and DragonFly™ catheters (LightLab Imaging, Inc.) at a pullback speed of 20 mm/s. A lesion was defined as the segment including frames with >0.5 mm maximal plaque thickness. When a vessel had multiple lesions, only one lesion containing the minimal lumen area site was selected and used for machine learning. After the exclusion of OCT frames at the branching sites, a total of 45,400 OCT frames (training set: 35,678 frames in 480 patients, test set: 9,722 frames in 122 patients) were included in the final model.

**Material and Methods.** Each OCT frame had a 0.4 mm interval and was labeled according to the presence or absence of TCFA. We defined OCT-derived TCFA as an OCT-delineated necrotic core with an angle ≥ 90° and an overlying FCT < 65 μm at the thinnest part to be the histologically defined threshold for detection.[1-4] Supplementary appendix summarizes the definitions of OCT findings and Supplemental Fig 1 provides the examples. All OCT images were analyzed by two independent investigators who were blinded to the information of the patients. In the event of discordance between the

readers, an assessment was obtained from a third independent investigator to determine a consensus. In the independent cohort including 65 OCT pullbacks, intra- and inter-observer variability between two independent observers (P.L. and S.L.) was evaluated to separate the frames with vs. without TCFA. The intra- and inter-observer and variability was assessed by kappa statistical analysis that corrected for the chance of simple agreement and accounted for systematic observer bias; a kappa > 0.80 indicated good agreement, and a kappa between 0.61 and 0.80 indicated moderate agreement. S.K, a cardiologist, reviewed annotated images, and supervised the whole steps of data preparation.

Supplementary appendix describes the densely connected convolutional networks (DenseNet)[19] and the used hyperparameters. The balanced amount of images with vs. without TCFA were randomly selected and used to train the model for each epoch. In the given number of TCFA-containing images, various augmentation techniques were utilized (Supplementary appendix).

Because a guiding catheter tip in the ostium may lead to a false diagnosis of TCFA at the proximal end of OCT image, we additionally conducted post-tuning of the model in separate 100 patients with 2590 OCT frames showing a guiding catheter to discriminate a TCFA-mimicking catheter from the ground truth.

The receiver operating characteristic (ROC) curve was based on the relative performance with consideration to the whole range of possible probability thresholds (from 0 to 1) and had an area ranging from “0.5” for classifiers without any prediction capability to “1” for perfectly classifying algorithms. Furthermore, a 5-fold cross-validation was used in each training process to flag overfitting (Supplementary appendix). The averaged performances were shown as mean ± standard deviations.

After the completion of cross-validation, the model was re-trained on the whole training dataset for a final prediction. The trained deep learning model provides a continuous number between zero and one for a referable classification of TCFA presence. The ROCs were plotted by varying the operating threshold, and the operating point with the largest area under a curve (AUC) value was selected. Fig. 1 shows the overall flow chart for the development of the deep learning model. The diagnostic performances at the frame level were assessed within the lesion and in the entire frames of an OCT pullback. With a batch size of 256, total computational time for analyzing an OCT pullback was calculated as the sum of data loading and inference time.

To evaluate the performance at the vessel level, percent-TCFA burden was calculated as the percentage of TCFA-containing frames in the total OCT frames within a vessel. Considering the potential clustering effect of multiple frames per vessel on the classification, the normalized diagnostic performances were calculated as the averages of the frame-level performances in each vessel (averaged sensitivity, averaged specificity and averaged overall accuracy). In addition, the performances in randomly selected 122 frames (including one frame per patient) in 122 test samples were calculated, and then the averaged performances of the independent 20 runs were shown as mean ±standard deviations.

To assess how much were overlapping between the predicted vs. the ground-truth TCFA frames in the test set, by using the definitions of true positive (TP), false positive (TP) and false negative (FN), Dice similarity coefficient (DSC) was calculated as 2TP / (2TP + FP + FN).

Gradient-weighted class activation mapping (Grad-CAM) was applied to the overall OCT frames that were classified as positive TCFA (supplementary appendix).

Ultimately, this process helped to clarify if the developed models utilized the histologically defined key features of TCFA (thin-cap overlying necrotic core) as the main target for detection.

## Results

**Clinical and lesion characteristics.** Table 1 shows a summary of the clinical characteristics of patients and quantitative coronary angiographic data. The overall frequency of OCT-defined TCFA in our sample was 7.3%. In the training sample (including 480 lesions with 35,678 frames), TCFA was detected in 2,577 (7.2%) frames. In the test sample (including 122 lesions with 9,722 frames), 717 (7.4%) frames had a TCFA. For the diagnosis of TCFA, intra- and inter-observer variability yielded moderate concordance (kappa =0.78 and kappa =0.74, respectively).

**Deep learning prediction of TCFA.** Table 2 summarizes the frame-level performance in terms of classifying frames averaged performances TCFA. The AUCs based on ROC analyses are also shown in Fig. 2. In the training samples, the deep learning model with 5-fold cross-validation showed an overall accuracy of 91.6 ± 1.7%, a sensitivity of 88.7 ± 3.4%, and a specificity of 91.8 ± 2.0% within the lesion (AUC 0.96 ± 0.01). In the test samples, the overall accuracy was 92.8% (AUC 0.96) within the lesion and 91.3% (AUC 0.96) in the entire pullback images (Table 2).

When the normalized diagnostic performances in vessel unit were assessed by averaging the frame-level performances for each vessel, the averaged sensitivity was 94.5±14.6%, the averaged specificity was 92.8±9.2%, and the averaged overall accuracy was 92.9±7.9%. In addition, the independent 20 runs by random sampling of one frame per patient in the 122 test samples showed the averaged sensitivity of 88.4±12.9%, the

averaged specificity of 93.7±1.9%, and the averaged accuracy of 93.3±1.9%.

Supplemental Table 1 shows a summary of frame-level performances based on the precision-recall curves of the training and test sets. In the test set, DSC between the predicted and the ground-truth TCFA frames was 0.73.

Among 112 TCFA lesions with at least two consecutive TCFA-containing frames, 103 (92.0%) were truly classified as 'positive' by the model. The length of the TCFA lesions classified as 'positive' (vs. 'negative') was significantly longer (6.8±6.7 frames vs. 2.0± 0.7 frames, $p<0.001$).

Fig. 3 shows the vessel-level performances in the test set. The predicted number of TCFA-containing frames within a vessel by the model was significantly correlated with the expert estimation ($r = 0.88$, $p < 0.001$). Furthermore, there was a significant correlation between percent-TCFA burdens per vessel as predicted by the model vs. by experts ($r = 0.87$, $p < 0.001$).

In the non-overlapping cohort including 65 OCT pullback images, the frame-level performances were tested in the entire pullback images. To classify frames with vs. without TCFA, the sensitivity, the specificity and the overall accuracy were 93.9%, 89.7% and 89.9%, respectively (AUC 0.97, Supplemental Table 2). In addition, the total computational time per an OCT pullback (including 344.1±76.2 frames) was 2.1 ± 0.3 seconds, which was much shorter as compared to the expert's interpretation (vs. 288.9 ± 269.9 seconds, $p<0.001$).

**Regions of attention.** In the test set, the localization maps were generated by Grad-CAM to demonstrate the regions of attention for predicting a TCFA (Fig. 4). In the region of attention, the red-coded area (>0.8) was localized at the site of the thin cap in 593 (93.4%) of the 635 frames that were assessed truly positive for TCFA by the model.

**False positive diagnosis.** In the test set, 616 frames were misclassified as a TCFA (false positive) and were subsequently reviewed by experts to identify the reasons. In 93.4% of those misclassified frames, the red-coded area was localized at a region mimicking a thin cap but was not determined as a TCFA because of the following reasons (Fig. 5): 1) the presence of fibrous tissue overlying calcification with an invisible abluminal border in 152 (24.6%) frames, 2) superficial infiltration of macrophages or microcalcification with back scattering in 108 (17.6%) frames, 3) a relatively thin fibrous cap that was not thin enough to meet the histological threshold of 65 μm in 106 (17.1%) frames, 4) an arc of signal-poor necrotic core less than 90° in 92 (14.9%) frames, 5) tangential signal loss caused by an eccentric catheter position or sidebranch opening in 71 (11.6%) frames, 6) a thin intimal layer facing the media of a normal vascular segment in 42 (6.8%) frames, 7) structures mimicking a TCFA caused by various artifacts including nonuniform rotational distortion and guide wire artifact in 41 (6.7%) frames, and 8) a signal-rich luminal border of red thrombus in 4 (0.7%) frames.

In Fig 3, 38 of 69 (55%) vessels without TCFA were misclassified as TCFA-containing vessels by the model. Among those with false positive diagnosis, 15 (40%) vessels did not have TCFAs that were detected at two or more consecutive frames. The predicted number of TCFA-containing frames within a vessel by the model was significantly correlated with the expert estimation ($r = 0.88$, $p < 0.001$, Fig. 3). Furthermore, there was a significant correlation between percent-TCFA burdens per vessel as predicted by the model vs. by experts ($r = 0.87$, $p < 0.001$).

**False negative diagnosis.** In the test set, 82 frames were misclassified as non-TCFA (false negative) and were also reviewed by experts. Among the misclassified frames, 64

(78%) frames were located adjacent to a TCFA-containing frame, thus suggesting that the false negative diagnosis frequently occurred at the transition zone between the frames with and without a TCFA.

## Discussion

We aimed to determine if a deep learning model could accurately predict the presence of a TCFA in OCT images. The main findings of the current study are as follows: 1) In the test samples, the overall accuracy for predicting a TCFA was 92.8% within the lesion and 91.3% in the entire pullback. 3) In the frames that are classified as TCFA, the activated map was localized at the site of the thin fibrous cap overlying the necrotic core in the majority.

Near-infrared light-based OCT has been the gold standard for the in vivo detection of TCFA because of the high spatial resolution and strong contrast between the lumen and vessel wall.[9-11] An ex vivo study reported a high level of inter-observer agreement between OCT- and histologically measured FCT. Conversely, the intra-class correlation coefficient for the in vivo measurement of FCT by OCT ranges from 0.48–0.56,[12-14] mainly because of the uncertainly in defining the necrotic core facing the border of the fibrous cap and macrophage infiltration, as well as imaging artifacts and other OCT features that may mimic a TCFA. Moreover, the quantification of TCFA by per-frame interpretation from a whole OCT pullback is time consuming. In this current study, inter-observer variability yielded moderate concordance (kappa =0.74), while the ML model consistently separated a TCFA vs. non-TCFA within only a few seconds per a whole pullback. Therefore, the development of an automatic algorithm based on standardized interpretation protocols is needed to reduce inter-observer variation and the

cost associated with OCT analysis.

Convolutional neural network is a category of deep neural networks, in which the connectivity pattern between neurons resembles the organization of the human visual cortex for recognizing patterns. By hierarchical processing with convolutional layers, the various activations of one neuronal layer is passed to the next layer, which allows the neural network to assemble more complex, higher level features. Several studies have proposed the automatic algorithms for OCT segmentation and plaque characterization. Rico-Jimenez et al. developed a computational method for automated atherosclerotic plaque characterization in 57 OCT cases.[20] To classify the OCT B-scans as the plaques with vs. without lipid, the overall accuracy was 85%. More recently, Abdolmanafi et al. developed a convolutional neural network that includes 26 OCT pullbacks to automatically classify the intima vs. medial layer of the coronary artery with an accuracy of 96%.[17] Gessert et al. also showed that convolutional neural networks trained on 49 patients identified atherosclerotic plaques with an accuracy of 91.7%.[18] However, the previous studies including only a small number of OCT did not predict the presence of TCFA, a prototype of vulnerable plaques.

Our deep learning model using 602 OCT cases quickly identified TCFA-containing frames in the entire pullback images, with a frame-level accuracy of 91.3%. Although deep learning is considered a "black box," the gradient-based Grad-CAM analysis provided a class-discriminative visualization map that highlighted a target region for prediction. The red-coded activation maps were localized to the thin-cap overlying lipid core in majority, thus indicating that this model could identify TCFA-containing lesions with good performance and with reasonable explanation.

This current model showed a negative predictive value of 99.0% for predicting a

TCFA-containing frames, but the positive predictive value (PPV) was only 50.8%. The false-positive cases were frequently associated with a signal-rich collagen band overlying a calcification with a poorly delineated abluminal border or a superficial radial shadowing caused by scattering macrophages or microcalcification. Considering that these findings mimicked a thin fibrous cap, it is sometimes a challenge even for clinicians to discriminate these features from a TCFA. In the setting of an eccentric catheter position or sidebranch opening, tangential signal dropout (as an imaging artifact that occurs when the light beam strikes the tissue under a glancing angle and travels almost parallel to the vessel wall) led to a misclassification of a stable plaque as a TCFA.[13] Therefore, to improve the PPV, the model needs to be further trained on prespecified subgroups of a larger cohort with the known OCT characteristics of calcification, macrophage infiltration, tangential signal drop, various extents of necrotic core, red thrombus, and imaging artifacts. Moreover, given that the expert's decision was affected by the contextual findings of the adjacent frames and the corresponding frame, training the deep learning model by using additional features obtained from adjacent frames may further improve the diagnostic performance.

**Limitations.** Given the low incidence of TCFA, the class imbalance may have affected the high rate of false positive diagnosis. Although the algorithm replicated the expert classification, the optimal threshold of OCT-measured cap thickness and the angular extent of TCFA still remain ambiguous. With a lack of external validation, the model requires studies of histological and clinical validation. Because the possibility of overfitting cannot be completely excluded, the model performances should be validated in a large prospective cohort. Although the normalized diagnostic performance and the averaged accuracy of 20 runs with one frame per patient were shown to be consistently

good, there may be a potential clustering effect of multiple frames per vessel.

**Conclusion.** Deep learning algorithm can accurately detect an OCT-TCFA with a high reproducibility. The time-saving computerized process may assist clinicians to easily recognize high-risk lesions and to make decisions in the catheterization laboratory.

## Impact on daily practice

- Deep learning algorithms can accurately identify the presence of a TCFA by detecting a thin cap.
- With an excellent per-frame and per-vessel performances, the model classified the lesions with and without TCFA in the entire pullback within a few seconds.
- This data-driven approach may assist clinicians to quickly recognize the high-risk coronary lesions.
-

- **Funding**

This study was supported by grants from the Korea Healthcare Technology R&D Project, Ministry for Health & Welfare Affairs, Republic of Korea (HI17C1080); the Ministry of Science and ICT (NRF-2017R1A2B4005886).

## Disclosures

The authors have no conflicts of interest to declare.

## References


1. Virmani R, Burke AP, Farb A, Kolodgie FD. Pathology of the vulnerable plaque. *J Am Coll Cardiol* 2006;**47**:C13–8.
2. Finn AV, Nakano M, Narula J, Kolodgie FD, Virmani R. Concept of vulnerable/unstable plaque. *Arterioscler Thromb Vasc Biol* 2010;**30**:1282-92.
3. Burke AP, Farb A, MalcomGT, Liang YH, Smialek J, Virmani R. Coronary risk factors and plaque morphology in men with coronary disease who died suddenly. *N Engl J Med* 1997;**336**:1276–82.
4. Virmani R, Kolodgie FD, Burke AP, Farb A, Schwartz SM. Lessons from sudden coronary death: a comprehensive morphological classification scheme for atherosclerotic lesions. *Arterioscler Thromb Vasc Biol* 200;**20**:1262–75.
5. Stone GW, Maehara A, Lansky AJ, de Bruyne B, Cristea E, Mintz GS, Mehran R, McPherson J, Farhat N, Marso SP, Parise H, Templin B, White R, Zhang Z, Serruys PW; PROSPECT Investigators. A prospective natural-history study of coronary atherosclerosis. *N Engl J Med* 2011;**364**:226–35.
6. Calvert PA1, Obaid DR, O'Sullivan M, Shapiro LM, McNab D, Densem CG, Schofield PM, Braganza D, Clarke SC, Ray KK, West NE, Bennett MR. Association between IVUS findings and adverse outcomes in patients with coronary artery disease: the VIVA (VHIVUS in Vulnerable Atherosclerosis) Study. *JACC Cardiovasc Imaging* 2011;**4**:894–901.
7. Yonetsu T, Kakuta T, Lee T, Takahashi K, Yamamoto G, Iesaka Y, Fujiwara H, Isobe M. Impact of plaque morphology on creatine kinase-MB elevation in patients with elective stent implantation. *Int J Cardiol* 2011;**146**:80-5.
8. Lee T, Yonetsu T, Koura K, Hishikari K, Murai T, Iwai T, Takagi T, Iesaka Y,

Fujiwara H, Isobe M, Kakuta T. Impact of coronary plaque morphology assessed by optical coherence tomography on cardiac troponin elevation in patients with elective stent implantation. *Circ Cardiovasc Interv* 2001;**4**:378-86.

9. Jang IK, Bouma BE, Kang DH, Park SJ, Park SW, Seung KB, Choi KB, Shishkov M, Schlendorf K, Pomerantsev E, Houser SL, Aretz HT, Tearney GJ. Visualization of coronary atherosclerotic plaques in patients using optical coherence tomography: comparison with intravascular ultrasound. *J Am Coll Cardiol* 2002;**39**:604-9.
10. Tearney GJ1, Brezinski ME, Bouma BE, Boppart SA, Pitris C, Southern JF, Fujimoto JG. In vivo endoscopic optical biopsy with optical coherence tomography. *Science* 1997;**276**:2037-9.
11. Ya Yabushita H1, Bouma BE, Houser SL, Aretz HT, Jang IK, Schlendorf KH, Kauffman CR, Shishkov M, Kang DH, Halpern EF, Tearney GJ. Characterization of human atherosclerosis by optical coherence tomography. *Circulation* 2002;**106**:1640-5.
12. Kim SJ, Lee H, Kato K, Yonetsu T, Xing L, Zhang S, Jang IK. Reproducibility of in vivo measurements for fibrous cap thickness and lipid arc by OCT. *J Am Coll Cardiol Img* 2012;**5**:1072–4.
13. Kini AS, Vengrenyuk Y, Yoshimura T, Matsumura M, Pena J, Baber U, Moreno P, Mehran R, Maehara A, Sharma S, Narula J. Fibrous Cap Thickness by Optical Coherence Tomography In Vivo. *J Am Coll Cardiol* 2017;**69**:644-57.
14. Goldstein BA, Navar AM, Carter RE. Moving beyond regression techniques in cardiovascular risk prediction: applying machine learning to address analytic challenges. *Eur Heart J* 2017;**38**:1805-14.
15. Krittanawong C, Zhang H, Wang Z, Aydar M, Kitai T. Artificial Intelligence in

Precision Cardiovascular Medicine. *J Am Coll Cardiol* 2017;**69**:2657-64.

16. Henglin M, Stein G, Hushcha PV, Snoek J, Wiltschko AB, Cheng S. Machine Learning Approaches in Cardiovascular Imaging. *Circ Cardiovasc Imaging* 2017;**10**:e005614.
17. Abdolmanafi A, Duong L, Dahdah N, Cheriet F. Deep feature learning for automatic tissue classification of coronary artery using optical coherence tomography. *Biomed Opt Express* 2017;**8**:1203-20.
18. Gessert N, Lutz M, Heyder M, Latus S, Leistner DM, Abdelwahed YS, Schlaefer A. Automatic Plaque Detection in IVOCT Pullbacks Using Convolutional Neural Networks. *IEEE Trans Med Imaging* 2018 doi:10.1109/TMI.2018.2865659.
19. Gao H, Zhuang L, Laurens van der M, Weinberger K. Densely connected convolutional networks, *IEEE Conference on Pattern Recognition and Computer Vision (CVPR)* 2017;4700-8.
20. Rico-Jimenez JJ, Campos-Delgado DU, Villiger M, Otsuka K, Bouma BE, Jo JA. Automatic classification of atherosclerotic plaques imaged with intravascular OCT. Biomed Opt Express. 2016;7:4069-85.F

F**igure legends**

**Central illustration.** Deep learning to classify the frames with vs. without OCT-TCFA.

**Figure. 1.** Flow chart of machine learning. TCFA=thin-cap fibroatheroma.

**Figure. 2.** ROC analysis. A: area under curves in the training set with 5-fold cross validation. B: area under curve in the test set.

**Figure. 3.** Vessel-level performances. A: The number of TCFA-containing frames per vessel as predicted by the model was significantly related to the expert-measured values. B. There was a significant correlation between the model-predicted %TCFA burden vs. expert- measured %TCFA burden.

**Figure. 4.** Activation maps using Grad-CAM technique. Two examples of TCFA-containing frames that were truly classified as a "TCFA" by the model. A. The red-coded area was localized at the site of the thin cap (white arrows) overlying the necrotic core (*). B. At the 10 o'clock direction, the red-coded area was localized at the region of the thin cap (white arrows) overlying the necrotic core (*). Conversely, at the 3–7 o'clock direction, a red-coded area was not seen. Although the red arrows indicate a signal-rich band that mimicked a thin cap, it overlies calcification and not a necrotic core. The white arrow heads clarify the abluminal border of calcification.

**Figure. 5.** Reasons for false-positive diagnosis. A. The red-coded area was localized to the fibrous tissue (arrow) overlying calcification with an invisible abluminal border

(arrow head). The presence of calcium was confirmed by experts reviewing the adjacent frames with a clear abluminal border. B. Superficial infiltration of macrophages (arrow) mimicked a thin cap but was associated with back scattering (arrow head) C. The thickness of the fibrous cap (arrows) was relatively thin but was less than 65 μm. D. Although the FCT (arrow) was 60 μm, the arc of the signal-poor necrotic core was less than 90°. E–F. The red-coded area was localized at the site of the tangential signal loss (arrows) caused by eccentric catheter position (E) and sidebranch opening (F). G. A thin intimal layer (arrows) facing the media (arrow heads) of a normal vascular segment mimicked a thin cap. H. The red-coded area was seen on the signal-rich surface of the guide wire (arrow). I. This near-normal segment was misclassified as TCFA by nonuniform rotational distortion as an imaging artifact. J. The red-coded area was localized on the signal-rich luminal surface of red thrombus (arrow).

**Table 1. Baseline characteristics in 602 patients with 602 coronary lesions**

| | |
|---|---|
| Clinical data | |
| Age, years | 65.5±9.7 |
| Men | 451 (75%) |
| Diabetes mellitus | 168 (28%) |
| Hypertension | 367 (61%) |
| Current smoker | 276 (46%) |
| Hyperlipidemia | 343 (57%) |
| Acute coronary syndrome | 162 (27%) |
| Quantitative angiographic data | |
| Involved vessel | |
| Left anterior descending artery lesion | 331 (55%) |
| Left circumflex artery lesion | 144 (24%) |
| Right coronary artery lesion | 187 (31%) |
| Diameter stenosis, % | 51.9±12.8 |
| Minimal lumen diameter, mm | 1.6±0.5 |
| Lesion length, mm | 17.5±10.4 |
| Proximal reference lumen diameter, mm | 3.4±0.5 |
| Distal reference lumen diameter, mm | 2.9±0.7 |

**Table 2. Frame-level performances based on ROC analyses to predict the presence of TCFA**

| | AUC[#] | Sensitivity (recall) | Specificity | PPV (precision) | NPV | Overall accuracy |
|---|---|---|---|---|---|---|
| Training sample (5-fold CV) | | | | | | |
| Group 1 | 0.962 | 88.3% | 93.3% | 51.4% | 99.0% | 93.0% |
| Group 2 | 0.951 | 85.6% | 91.3% | 43.8% | 98.8% | 90.8% |
| Group 3 | 0.967 | 85.4% | 94.5% | 55.2% | 98.8% | 93.8% |
| Group 4 | 0.971 | 90.7% | 90.6% | 43.4% | 99.2% | 90.6% |
| Group 5 | 0.966 | 93.3% | 89.5% | 41.5% | 99.4% | 89.8% |
| Averages in 5 groups* | 0.963±0.008 | 88.7±3.4% | 91.8±2.0% | 47.1±5.9% | 99.0±0.3% | 91.6±1.7% |
| Test sample | 0.962 | 88.6% | 93.2% | 50.8% | 99.0% | 92.8% |

CV=cross-validation, PPV=positive predictive value, NPV=negative predictive value

[#] area under the curves based on the receiver operating characteristic (ROC) analysis

*Average of 5-fold cross-validation in the training sample

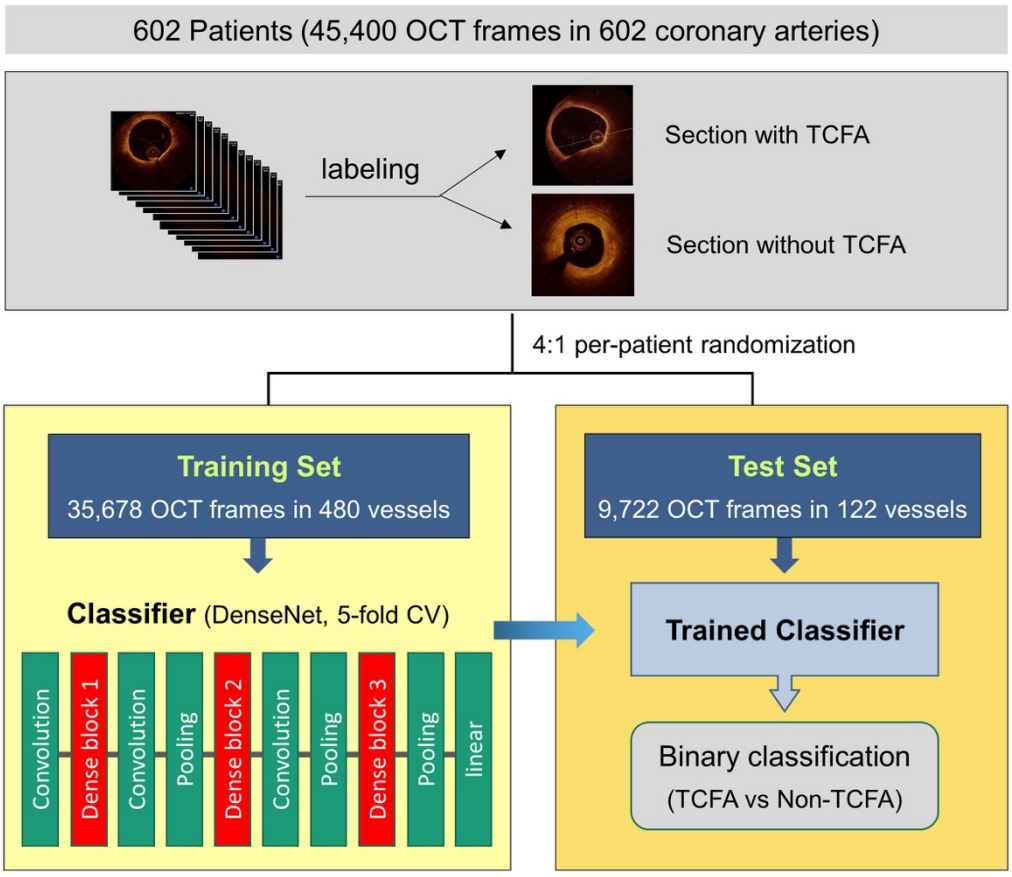

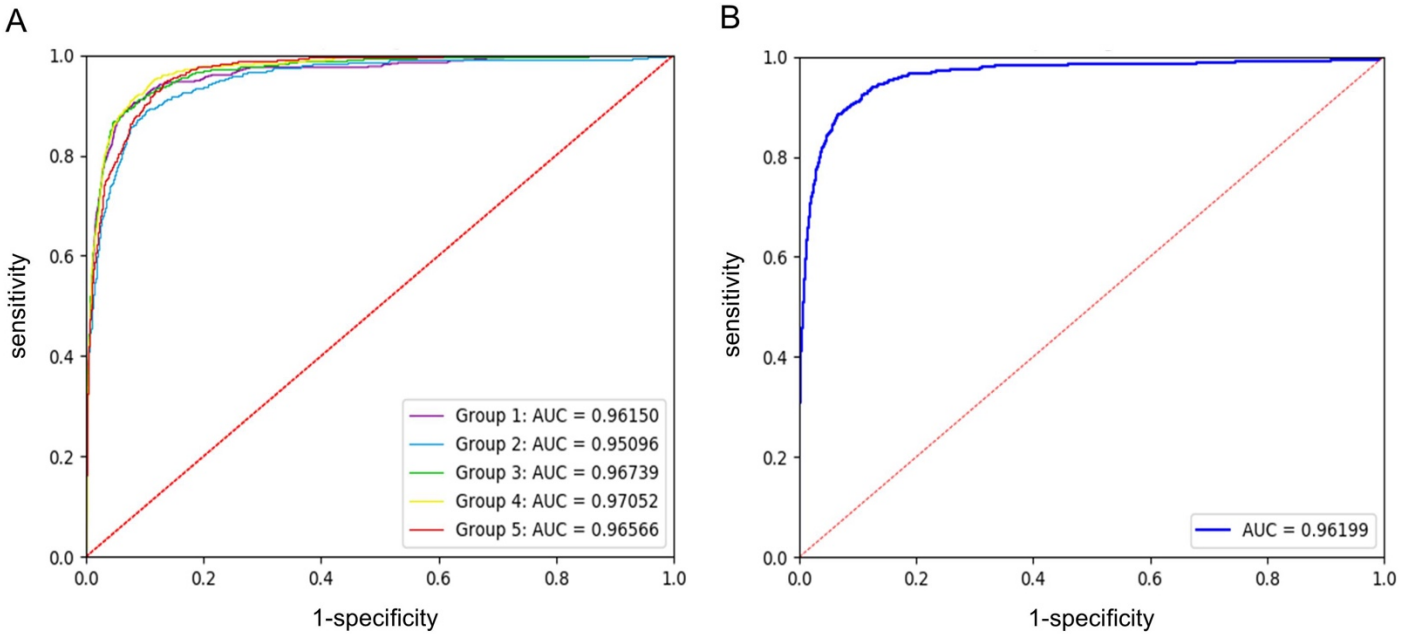

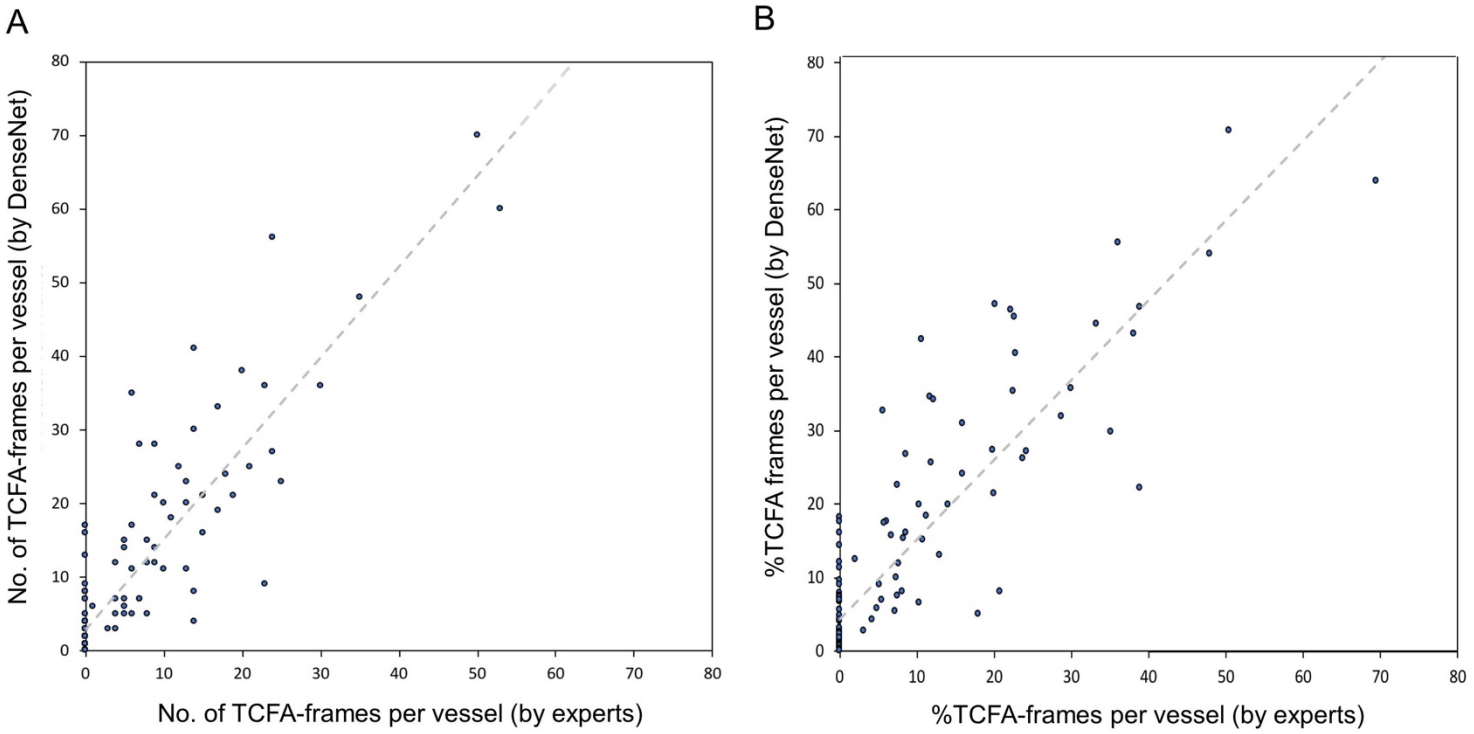

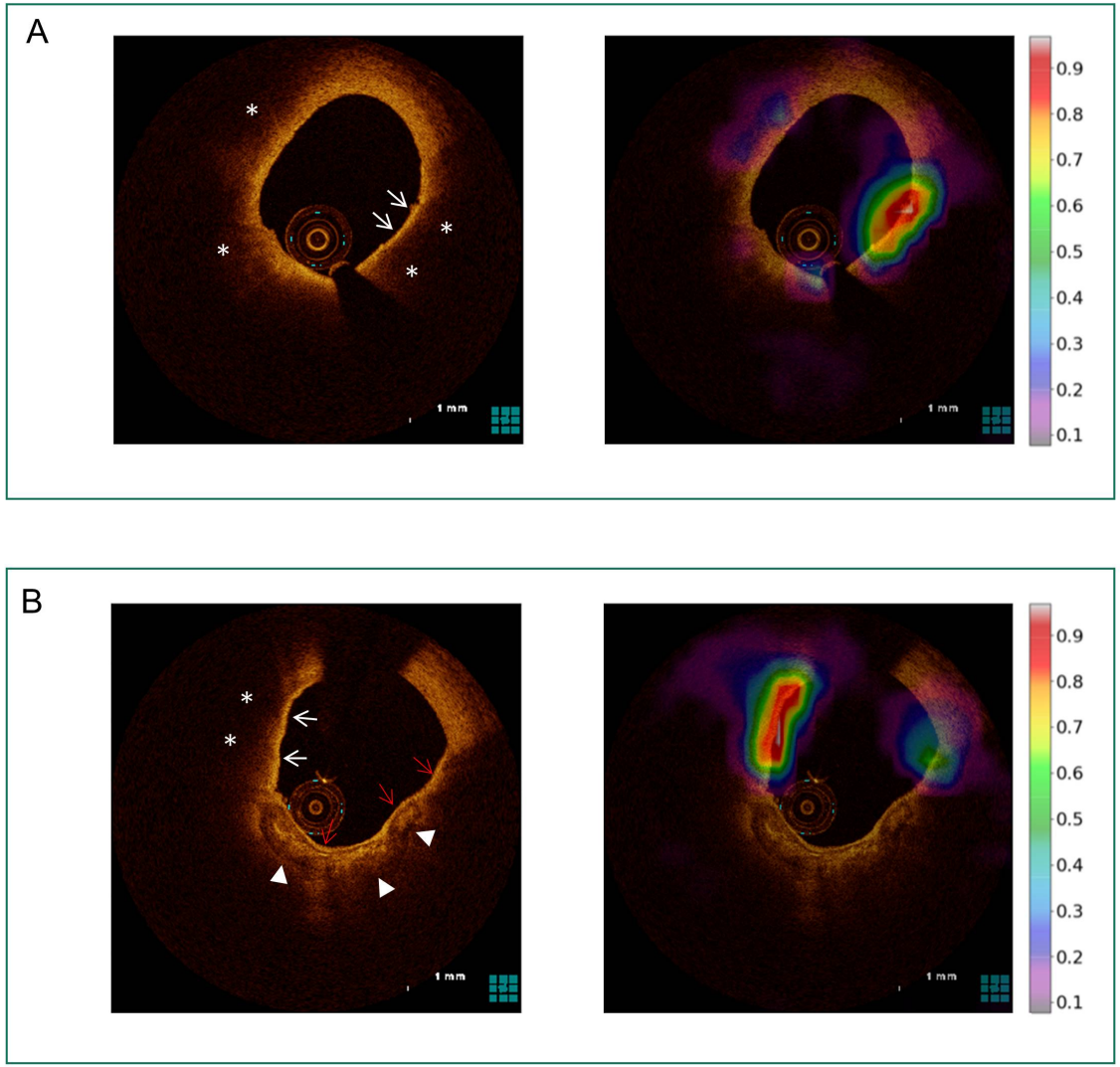

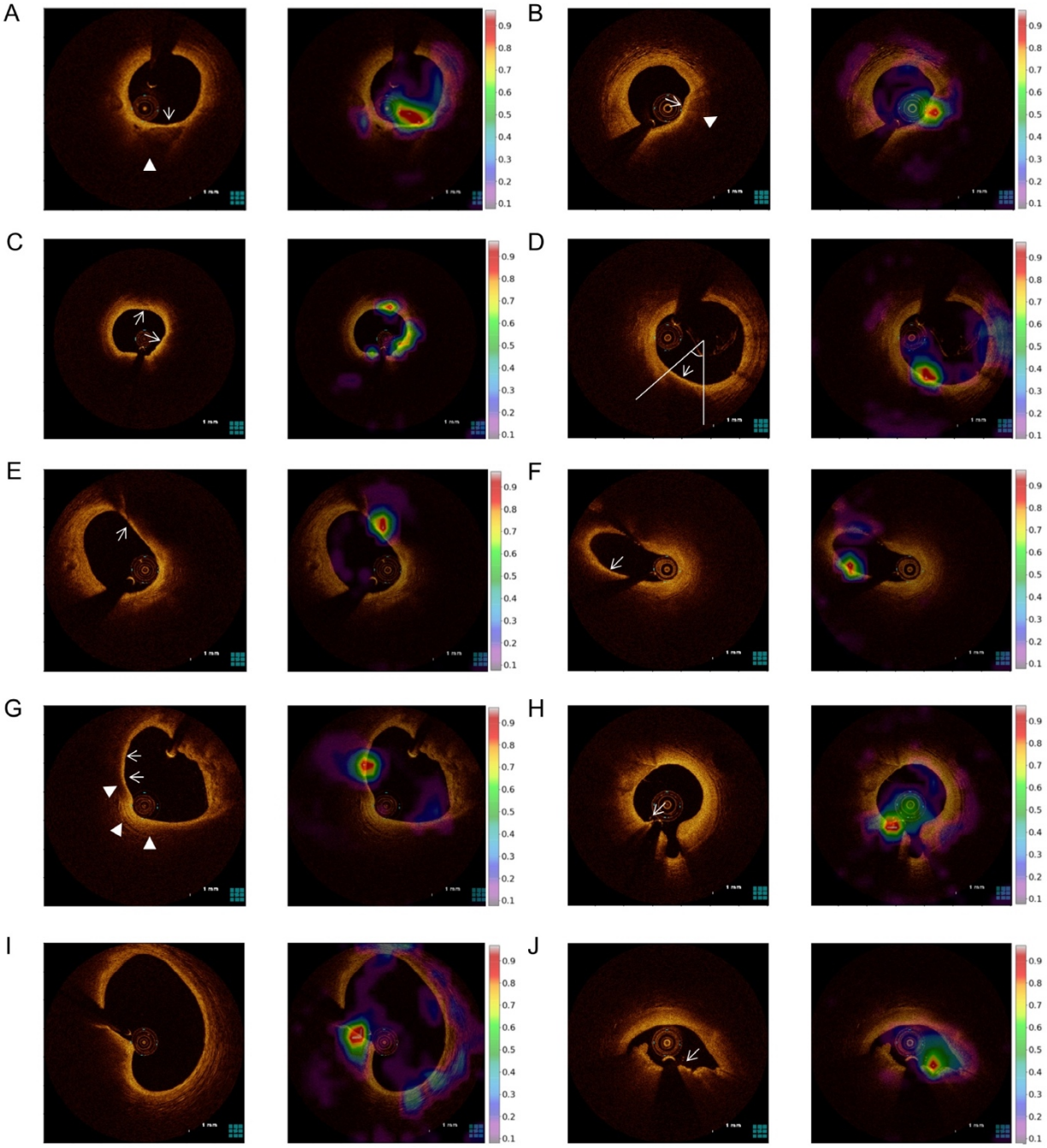

# SUPPLEMENTAL MATERIAL

**Definitions of OCT findings**.

Although both the necrotic core and calcification were characterized by a signal-poor region, they were discriminated by the diffuse vs. sharp margins of the signal-poor area, respectively. Macrophage accumulation was defined as a signal-rich punctate region with tail shadows in the deeper layer behind the superficial band of macrophages. When the abluminal border of the signal-poor region was unclear, a series of adjacent frames was carefully reviewed. Supplemental Fig 1 shows the examples of the OCT finding. All OCT images were analyzed by two independent investigators who were blinded to the information of the patients. In the event of discordance between the readers, an assessment was obtained from a third independent investigator to determine a consensus.

**5-fold cross validation**.

Cross-validation is a model validation techniques for assessing how the results of an analysis will generalize to an independent data set. It is commonly used in applied machine learning to compare and select a model for a given predictive modeling problem. In K Fold cross validation, the data is divided into k subsets and train the model on k-1 subsets and hold the last one for test. This process is repeated k times, such that each time, one of the k subsets is used as the test set/validation set and the other k-1 subsets are put together to form a training set. In the current study, 5-fold cross validation scheme divided the training sample into non-overlapped five partitions. Each partition was rotated to be the test set and the rests are used as training data. The

accuracy was calculated by averaging the accuracies over five tests.

**Deep learning model**.

Convolutional neural networks are composed of multiple building blocks such as convolution layers, pooling layers, and fully connected layers and are designed to automatically and adaptively learn the spatial hierarchies of features by using a backpropagation algorithm. We used the densely connected convolutional networks (DenseNet) model, which connects each layer to every other layer in a feed-forward fashion. To discriminate OCT frames without or with TCFA, all layers of the DenseNet model were fine-tuned by backpropagation via the whole net. Binary cross entropy with logits loss was used for loss function to optimize the prediction model. Furthermore, an Adam optimizer was applied with an initial learning rate of 0.0002. Considering the possibility of overfitting in the given number of TCFA-containing images, various augmentation techniques such as crop, random rotation, elastic transformation, horizontal and vertical flip, and use of Gaussian filters were utilized.



**Grad-CAM**

To support visual explanations for predicting the presence or absence of TCFA via deep learning-based models, we used gradient-weighted class activation mapping (Grad-CAM), which is a recently proposed network visualization technique. By utilizing the gradients to estimate the importance of the spatial locations of convolutional layers, Grad-CAM produced a localization map that highlighted the attended regions on the OCT image to predict TCFA. The threshold > 0.8 (coded as red) was considered to be the key area of attention.

**Supplemental Table 1. Frame-level performances based on the precision-recall curves to predict a TCFA**

| | AUC | Sensitivity (recall) | Specificity | PPV (precision) | NPV | Overall accuracy |
|---|---|---|---|---|---|---|
| Training set with 5-fold CV | | | | | | |
| Group 1 | 0.78 | 0.73 | 0.98 | 0.72 | 0.98 | 0.95 |
| Group 2 | 0.72 | 0.65 | 0.98 | 0.70 | 0.97 | 0.95 |
| Group 3 | 0.78 | 0.78 | 0.97 | 0.64 | 0.98 | 0.95 |
| Group 4 | 0.73 | 0.66 | 0.98 | 0.75 | 0.97 | 0.96 |
| Group 5 | 0.74 | 0.71 | 0.97 | 0.65 | 0.98 | 0.95 |
| Averages in 5 groups* | 0.75 ± 0.03 | 0.70±0.05 | 0.97± 0.01 | 0.69± 0.04 | 0.98±0.01 | 0.95± 0.01 |
| Test set | 0.80 | 0.71 | 0.98 | 0.75 | 0.98 | 0.96 |

AUC=area under the curve, CV=cross-validation, PPV=positive predictive value, NPV=negative predictive value

*Average of 5-fold cross-validation in the training samples

**Supplemental Table 2. Frame-level performances in the non-overlapping cohort including 65 OCT pullback images**

| | AUC | Sensitivity | Specificity | PPV | NPV | Overall accuracy |
|---|---|---|---|---|---|---|
| ROC-based analyses | 0.97 | 0.94 | 0.90 | 0.28 | 0.99 | 0.90 |
| Precision-recall curve-based analyses | 0.65 | 0.79 | 0.96 | 0.48 | 0.99 | 0.96 |

AUC=area under the curve, CV=cross-validation, PPV=positive predictive value, NPV=negative predictive value

*Average of 5-fold cross-validation in the training sample